Flux and energy analysis of species in hollow cathode magnetron ionized physical vapor deposition of copper

L. Wu,[1] E. Ko,[1] A. Dulkin,[1] K. J. Park,[1] S. Fields,[1] K. Leeser,[1] L. Meng,[2] and D. N. Ruzic[2]
[1]*Novellus Systems, Inc., 4000 North 1st St., San Jose, California 95134, USA*
[2]*Center for Plasma-Material Interactions, University of Illinois at Urbana-Champaign, 201 South Goodwin, Urbana, Illinois 61801, USA*

(Received 3 August 2010; accepted 29 September 2010; published online 3 December 2010)

To meet the stringent requirements of interconnect metallization for sub-32 nm technologies, an unprecedented level of flux and energy control of film forming species has become necessary to further advance ionized physical vapor deposition technology. Such technology development mandates improvements in methods to quantify the metal ion fraction, the gas/metal ion ratio, and the associated ion energies in the total ion flux to the substrate. In this work, a novel method combining planar Langmuir probes, quartz crystal microbalance (QCM), and gridded energy analyzer (GEA) custom instrumentation is developed to estimate the plasma density and temperature as well as to measure the metal ion fraction and ion energy. The measurements were conducted in a Novellus Systems, Inc. Hollow Cathode Magnetron (HCM^{TM}) physical vapor deposition source used for deposition of Cu seed layer for 65–130 nm technology nodes. The gridded energy analyzer was employed to measure ion flux and ion energy, which was compared to the collocated planar Langmuir probe data. The total ion-to-metal neutral ratio was determined by the QCM combined with GEA. The data collection technique and the corresponding analysis are discussed. The effect of concurrent resputtering during the deposition process on film thickness profile is also discussed. © *2010 American Institute of Physics*. [doi:10.1063/1.3504371]

I. INTRODUCTION

Copper barrier and seed layers used in the formation of metal wires in VLSI interconnects have traditionally been deposited by neutral-dominant sputter deposition, also referred to as physical vapor deposition (PVD), and for roughly the last decade by ionized physical vapor deposition (iPVD). The latter employs both metal and gas ions, not only for the target sputtering but also for the film formation. iPVD has become the predominant approach to the fabrication of copper interconnects, due to its capability to deposit highly conformal, low overhang films in small features.[1] The fundamental physics of the dc gas discharge plasma used for metal target sputtering is well understood and has been studied both analytically and experimentally with numerous plasma diagnostic techniques. There are several commercial iPVD sources currently in production and a number of prospective sources in development capable of producing high metal ion fraction of the sputtered target material. To ensure uniform, engineered film characteristics across the substrate, one must transfer the ions from the source area to the substrate in a controlled fashion. This objective can be achieved only if all components of the deposition flux, namely, metal neutrals and ions as well as gas ions, have spatially uniform distribution. The other fundamental parameter of the deposition process is the energy of the depositing species, which in iPVD can be controlled due to the presence of the high ion fraction. These ions in the flux impinging the wafer not only affect kinetics of deposition but also cause sputtering of the deposited film if they carry sufficient energy. The above mentioned advances in iPVD source design require a new round of plasma studies, with the emphasis on measuring deposition flux characteristics.

Since the ion flux and energy affect both the film deposition and sputtering rates as well as the in-feature performance, a fundamental understanding of metal ion fraction, ion energy, and plasma characteristics is critical for advanced iPVD process development. Computer simulation has been widely used for plasma modeling; however, these models generally have difficulty predicting the on-wafer plasma characteristic for complicated iPVD systems.[2–4] Therefore, direct characterization of the wafer level ionization fraction, ion energy distribution (IED), and other key plasma characteristics is required. Several classes of plasma diagnostic techniques, falling roughly into three categories, have been successfully used for general plasma studies: electrical, optical, and mass spectroscopy. Each has advantages and disadvantages, and usually several diagnostics have to be combined to obtain key plasma characteristics for iPVD. In particular, absorption spectroscopy and energy-resolved mass spectrometry have been developed for metal ion fraction measurement.[5–7] However, the absolute ion fraction from the spectral data is often found to be inaccurate because of many unknown collisional cross-sections of low ionization states and significant deviation of the electron energy distribution from a Maxwellian distribution.[8] In addition, a typical mass spectrometer with its differential pumping hardware requires substantial space, which makes adaptation to a production iPVD system difficult. Laser-induced fluorescent analysis is another example of a precision diagnostic,

which can measure both particle concentrations and their velocities, but requires substantial space around the plasma vessel.

An *in situ* ion fraction and ion energy distribution measurement can be realized by a quartz crystal microbalance (QCM) combined with a gridded energy analyzer (GEA).[9–12] GEA has been employed to study ion energy distribution in various RF discharge systems.[13–15] Bohm addressed problems arising from poor analyzer design, particularly with respect to the choice of grid material and dimensions.[16] With appropriate modification, the GEA has also been used to determine ion angular distribution in different reactors.[17,18] Rossnagel and Hopwood introduced the QCM in the inductively coupled RF plasma to measure the deposition rate of metal fluxes.[9,10] However, their design was only useful at low plasma densities due to the issues with plasma penetration. Green *et al.* built similar instruments and improved the performance by employing a three-grid GEA to reduce the plasma penetration and biasing the QCM at the potential of the substrate.[11] The ionization fraction was further calibrated by considering the shadowing effect of GEA geometry.[11] However, none of these techniques have been used to map out the on-wafer characteristics of a high power 300 mm commercial iPVD system. Moreover, those tools were usually placed on top of the wafer, which would likely perturb the film-forming plasma. In this paper we present a custom QCM/GEA system enabling the nonperturbing ion fraction measurement with substrate spatial resolution appropriate for a 300 mm HCM module.

Langmuir probes, one of the earliest and most basic of plasma diagnostics, have been used in a wide variety of plasmas ranging from low temperature plasmas to leading edge fusion research plasmas.[19–21] The probe's current–voltage (IV) curves, which can be obtained from simple experimental setup, indicate many plasma characteristics, such as plasma potential, electron density, electron temperature, and floating potential.[22] One drawback to the method is that data interpretation is often complicated due to perturbation of the subject plasma by the probe itself. Extensive study of Langmuir probe characterization has been reported for various plasmas in the literature.[23–26] Most Langmuir probe diagnostics for PVD systems have been focused on either target sputtering plasma or plasma diffusion and transport.[27–29] However, it is the on-wafer plasma characteristics that directly impact the film in-feature performance. Therefore, such on-wafer plasma diagnostics are more explicit and helpful for process optimization. In studying conductive thin film deposition, the metallic film can easily bridge insulating probe components, hence significantly reducing probe lifetime and compromising the measurement repeatability. In response, a set of novel planar probes is designed to map out the on-wafer plasma characteristics in a commercial 300 mm deposition system.

This paper demonstrates a novel method combining QCM, GEA, and a planar Langmuir probe with data collected from an iPVD Cu process. The plasma density, electron temperature, ion flux, metal ion fraction, and ion energy are characterized for iPVD Cu deposition on a 300 mm wafer inside a Novellus HCM^{TM} source.

II. APPARATUS

The custom instrument is integrated into a modified wafer pedestal such that the surface of the instrument is coincident with the simulated substrate surface. In addition, the apparatus includes features simulating the critical geometry and materials at and about the edge of an actual pedestal. This arrangement results in measurements coincident with the wafer, with minimal perturbation to the film-forming plasma. A physical array of sensors in the instrument at three discrete locations representing the center, midradius, and edge of the wafer provided spatial resolution which allowed us to obtain information about radial distribution of the fluxes and energies across the substrate.

A. QCM/GEA setup

QCM/GEA modules are located at the center (0 mm), midradius (75 mm), and edge (150 mm) of the QCM pedestal [Fig. 1(a)]. Each GEA consists of three grids separated by ceramic rings and is positioned directly above a QCM [Fig. 1(b)]. Three ceramic disks provide sturdy support for the grids while insulating the grids from each other. Each grid spans a 22.2 mm diameter hole that extends from the top surface of the instrument through the centers of the ceramic disks down to the QCM crystal. Grids are made from stainless steel mesh fabric. Four different mesh wire dimensions have been tested. The wire diameters were 0.065 ± 0.004, 0.089 ± 0.004, 0.165 ± 0.01, and 0.229 ± 0.01 mm, and the grid spacings were 0.102, 0.181, 0.629, and 1.359 mm, respectively. The grid transparencies were 37%, 45%, 63%, and 73%. The distance between the top and middle grids was 3.2 mm. The distance between bottom and middle grids was 2.7 mm. The distance from the QCM crystal surface to the top grid was 9.8 mm. The water-cooled QCM made by Sycon

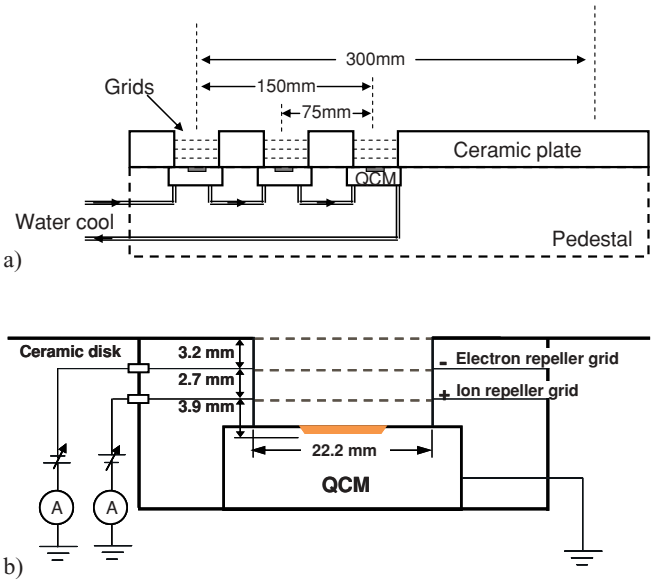

FIG. 1. (Color online) (a) Cross-sectional schematic view of the center, midradius, and edge QCM/GEA stations on a modified 300 mm pedestal. (b) A schematic representation of the QCM and GEA station and electric potential configuration.

Instruments is electrically connected to the grounded pedestal.[30] It transmits a signal through a vacuum feedthrough to the offboard data acquisition and analysis system, which processes the data and calculates and displays the accumulated deposition mass among other parameters. Mechanically the instrument was fully compatible with the regular wafer transfer in and out of the module. It allowed a shutter wafer placed on the top of the ceramic plate to prevent unwanted deposition during target burn-in and conditioning, which is required in PVD after chamber exposure to atmosphere.

B. Langmuir probe array

Under the heavy deposition encountered in a production PVD reactor, without proper mitigation the deposited metal film could easily bridge probe and other noncurrent collecting components, severely limiting the probes' lifetime and accuracy. In this apparatus, a novel probe design, as shown in Fig. 2(a), is employed to overcome this issue and as a result, the probes can be used for a considerably long period without sacrificing the performance. The apparatus is composed of probes, guard rings, holders, and top and bottom ceramic plates. In order to manage film flaking, which could result in electrical shorts or alter effective electrode areas, all the horizontal surfaces that are directly exposed to process are grit blasted to increase surface roughness and improve adhesion. Surfaces between conductive components are coated with arc-sprayed aluminum oxide to electrically isolate them. The T-shaped probe geometry additionally prohibits any unwanted electrical connection between the probe and the guard ring. A guard ring is used in conjunction as part of the probe assembly. The guard ring is biased at the same potential as the planar probe, which ensures the uniform sheath potential across the probe.[31] The gap between the probe and the guard ring is 0.25 mm, which is shorter than the nominal sheath length of approximately 0.4 mm, and the gap between guard ring and holder is 0.5 mm, which is intentionally designed to be greater than the nominal sheath length. Figure 2(b) shows an isometric view of the Langmuir probe array. A total of 24 probes are distributed across a ceramic plate that resembles a 300 mm wafer. The first set of nine probes collects a first line scan across the simulated wafer, with the locations corresponding to those for sheet resistance (Rs) measurements for blanket wafer test. The second line scan, which includes a central station common with the first set, is located 80° rotated from the first line array. This seemingly arbitrary rotation is dictated by the six lift pin locations that are located every 60° in the reactor. These two lines scans are separated enough to indicate overall on-wafer-level plasma characteristics. A total of 11 probe stations inclusive of four common with the first two line arrays are distributed circumferentially every 40° or 20°. These edge locations are designed to match 3 mm edge exclusion used by Rs metrology tools, and 11 locations are sufficient to capture edge effects, if any. Only center, middle radius, and edge probe results are presented in this paper because they represent plasma characteristics across the wafer. During target burn-in and conditioning processing in the reactor, four short mesas are employed to support the shuttering wafer and prevent direct contact between wafer and probes.

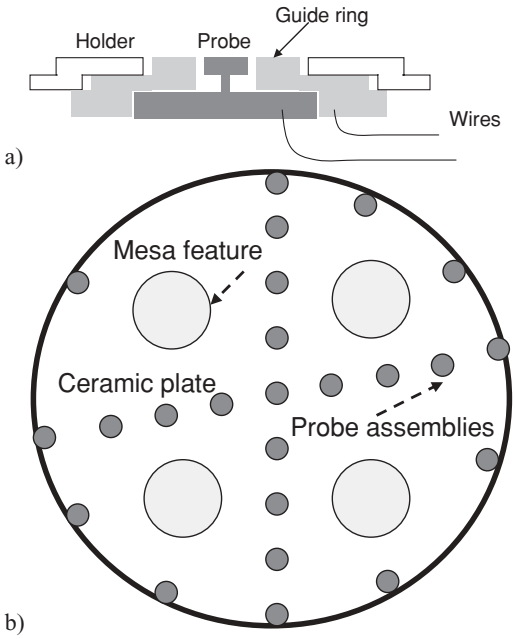

FIG. 2. (a) Schematic view of a single probe assembly. The central component is the collector probe, surrounded by a voltage biased guard ring, centered and shielded by an insulator. Between the components are high aspect ratio labyrinth features to prevent bridging by sputtered, conductive thin films. Except for the top surface of the metallic probe and guard rings, all other surfaces are insulated with arc-sprayed aluminum oxide. (b) Schematic view of complete Langmuir probe array, totaling 24 probes distributed on a ceramic plate. Four mesa features support a wafer during target burn-in processing.

III. QCM/GEA CALIBRATION

A. GEA bias

In a standard QCM configuration, the deconvolution of neutral and ion deposition can be achieved by varying grid bias.[11] As electron current cannot be readily distinguished from ion current and as such taints the ion current data, it is necessary to float the top grid to prevent electrons from penetrating. The middle grid bias (V_m) and bottom grid bias (V_b) have a negligible effect on the top grid floating potential. Less than 1 V dc of top grid floating potential variation was observed over a wide range (−100 to 40 V) of middle and bottom grids bias combinations, indicating that the incoming charged species' fluxes entering the GEA remain approximately constant regardless of the applied grid biases. Figure 3 shows the electron and ion current collected by the middle and bottom grids as well as the total current on these two grids. The top grid is floated at –40 V, the middle grid is biased at −50 V, and the bottom grid bias scans from 40 to −100 V. In this configuration, the middle grid collects ions since its potential is lower than the top grid floating potential. When the bottom grid is biased less than −50 V, ions are electrostatically attracted by the bottom grid due to the electrical field. These data indicate that approximately 34% of the ions are collected by the bottom grid, which agrees well with the

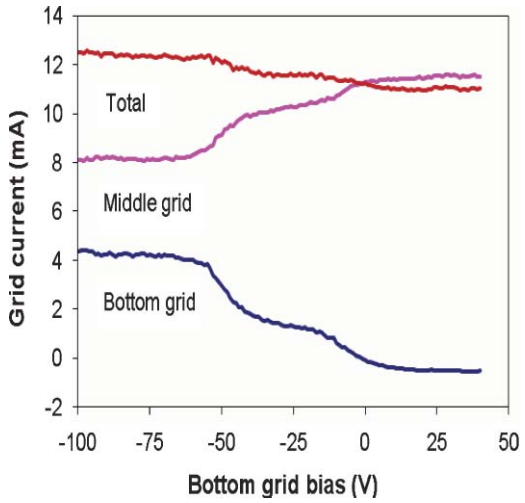

FIG. 3. (Color online) Current collected from middle and bottom grids. The top grid is floating, the middle grid is biased at –50 V, and the bottom grid is scanned from 40 to –100 V. The total current collected by middle and bottom grids remains roughly constant.

effective collector area which is calculated to be roughly 31% based on grid transparency. The error is attributed to a small amount of electron current collected by the positively biased bottom grid. Those electrons are the secondary electrons emitted from the sputter target. After being accelerated by the dc plasma sheath voltage, most secondary electrons from the target collide with background gas and metal species to generate high density HCM plasma. A portion of these high energy electrons can overcome the 50 V potential barrier and arrive at the wafer surface with no or few collisions because of low ($\sim 1 \times 10^{-4}$ Torr) process pressure.

After acceleration across the sheath potential, ions are reasonably collimated in the direction perpendicular to the grid surface.[32] Both neutrals and ions reach the QCM/GEA when grids are biased at potentials lower than the floating potential. Only neutrals can reach the QCM when the bottom grid is positively biased with respect to the plasma potential, V_p. As such, the ion fraction can be determined by the metal fluxes received at two different potential configurations, which need to be carefully chosen to produce accurate results. First of all, the negative grid bias should not be so low that the ions gain sufficient energy to sputter the grid, which would result in overestimation of the neutral flux and in turn underestimation of the actual ion fraction. Second, the positive grid bias should be high enough to repel all high energy metal ions; otherwise the ion fraction will be underestimated. For these reasons, various grid potential configurations were tested to identify the optimum and obtain a robust operating condition.

Figure 4 shows different grid potential zones within the QCM mass deposition profile. In zone 1, the middle grid bias is higher than V_p and ions cannot reach the QCM. In zone 2, grid sputtering occurs due to the high negative bias, which leads to higher apparent QCM deposition rate. Zone 3 has robust neutral deposition because the bottom grid is positive enough to repel all the ions. Zone 4 has robust neutral and ion deposition without grid sputter. For the data reported in this paper, the V_m is 10–30 V lower than V_f. The V_b is 10–20 V lower than V_m when collecting both ions and neutral atoms, and 90–120 V higher than V_m when collecting neutral atoms only.

B. Grid dimensions

The top grid mesh aperture size should be at most equal to the plasma sheath thickness to prevent plasma penetration and to reduce sheath potential disturbance across the aperture. For plasma with an electron density (n_e) of 10^{11} cm^{-3} and electron temperature (T_e) of 4 eV, the sheath thickness is approximately 188 μm. Since the grid's electrical field affects the ion energy gained through the sheath, the grid aperture should not disturb the potential variation in the sheath.[15] It is often argued that the aperture dimension is required to be smaller than sheath dimensions in order to minimize sheath potential variation. Edelberg *et al.* suggest that significant sheath

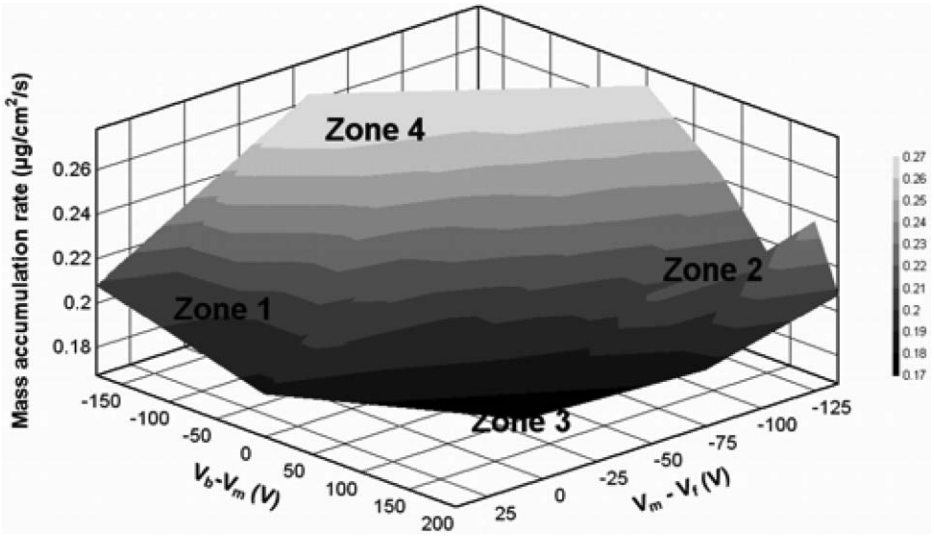

FIG. 4. Contour plot of the QCM mass accumulation rate as a function of grid bias. The $V_m - V_f$ is the potential difference between the middle grid and V_f. The $V_b - V_m$ is the potential difference between the bottom grid and middle grids.

TABLE I. Effects of GEA grid dimension on QCM results.

Mesh aperture (μm)	102	181	629	1359
Grid transparency (%)	37	45	63	73
Geometry factor	0.68	0.58	0.39	0.43
Ratio of ion fraction (normalized to 181 μm grid)	1.12	1	0.76	0.36

potential distortions are presented at the calculated sheath size.[15] The field distortion is only minimized when the grid size approaches the Debye length. Furthermore, the grid wire size must be large enough to thermally conduct collision-induced power out of the grid. Unfortunately, very small mesh aperture dimension and excessively large wire size result in low transparency, which limits the QCM mass flux and GEA ion signal, and hence degrades the signal-to-noise ratio.

In order to optimize grid dimension, a few grids with different dimensions have been tested in a low plasma density process. As shown in Table I, 1359 μm mesh size is much larger than the sheath size. Hence, the positively biased grid could not repel all the ions, leading to smaller metal ion fraction. As the mesh size approached the sheath size, the ion fraction gradually saturated. The transparency of the each grid is 45%, giving a total accumulated transparency of 9% after three layers of grids, which provides signals high enough to be detected by QCM. Although further reduction in mesh size lowers the signal-to-noise ratio, larger errors result compared to the other mesh sizes. The sheath potential profiles on different grids also affect the measured ion energy distribution, as the sheath potential disturbance can cause some ions to lose partially or entirely their momentum in the direction perpendicular to the grid surface.[16]

To guarantee proper analyzer operation, the gap between the top grid and the QCM crystal (l) needs to be smaller than the mean free path of ions for resonant charge exchange collisions (λ_{CX}), e.g., $Ar^+_{fast} + Ar_{slow} \rightarrow Ar_{fast} + Ar^+_{slow}$.[16] The HCM experimental pressure is less than 1 mTorr, in which the ion collision mean free path λ (even shorter than λ_{CX}) is 5.8 cm for room temperature Ar gas. In this QCM design, the distance between the top grid and the QCM crystal was 9.8 mm, which satisfies this requirement. GEA mesh material selection is also critical to address several material properties of interest. Sputter yield should be low to provide sufficient resistance to sputtering, especially for the top grid. In order to prevent sagging of the grid, which would result in distortion of electric fields and grid electrode areas, thermal conductivity should be sufficiently large, coefficient of thermal expansion should be low, and creep resistance should be appreciable.

C. Geometrical correction factor

Since the QCM sensor is located at the bottom of the GEA's cylinder well, the incident neutral atoms impinging at a large angle are shadowed by the wall so that only a certain fraction of neutrals entering GEA actually arrive at the QCM. This fraction, defined as the geometrical correction factor, was found to be dependent on the dimensions of the energy analyzer as well as the gas pressure, which affects the distribution of neutral atoms. The ions, however, are assumed to be well collimated by the electric field so that the geometrical correction factor for ions is unity. The geometrical correction factor for neutrals has to be considered to calibrate the metal ion fraction. Green *et al.* calculated the geometrical correction factor as a function of the QCM characteristic dimension based on the solid angle.[11] Application of this method results in a theoretical geometrical factor of 0.58 for this QCM configuration. Based on the on-wafer growth rate, the expected QCM deposition rates are calculated for a geometrical correction factor of 1. Since the actual deposition rate on the QCM is lower because of the loss of neutral the difference between actual QCM and on-wafer deposition rates can be employed to estimate the geometrical correction factor. As shown in Table I, for the 181 μm grid the geometrical factor is 0.58, agreeing with the theoretically expected value. For 1359 μm mesh sizes, a large fraction of ions is not collimated by the electric field. Like neutral atoms, the ions impinging at a large angle are shadowed by the wall, which results in underestimation of the metal ion fraction.

IV. EXPERIMENTAL RESULTS

Comprehensive studies of iPVD HCM Cu deposition process have been conducted using the discussed data collection system. Typical measurement results of plasma parameters, ion fluxes, and ion energies are presented below. The detailed correlation with the film step coverage, morphology, etc., will be discussed elsewhere.[33]

A. Metal ion fraction and Ar^+/Cu^+ ratio

Metal ion fraction is defined as the ratio of metal ions to the sum of metal ions and metal neutrals in the deposition flux:

$$\text{Ion fraction} \equiv \frac{M^+}{M^0 + M^+}.$$

Ar^+/Cu^+ ratio is defined as the ratio of Ar ions to Cu metal ions. They were measured at the center, midradius, and edge positions. The results presented here are normalized by the center QCM data due to the sensitivity of process information. The error bar was calculated from the multiple measurements at different times by different operators. As shown in Fig. 5(a), the copper ion fraction at the center of the wafer is approximately 15% higher than that at the edge of the wafer. The Ar^+/Cu^+ ratio is constant across the wafer, which suggests that Ar ions and Cu ions follow the same trajectory under the influence of electrical and magnetic fields.

B. Ion energy distribution

The metal ion fraction, the amount of total ion species hitting the wafer, and the ion energy determine the in-feature performance, such as step coverage and overhang.[32] The ion energy without any induced bias on the wafer is indicative of the plasma characteristics inside the source plasma. Most ions

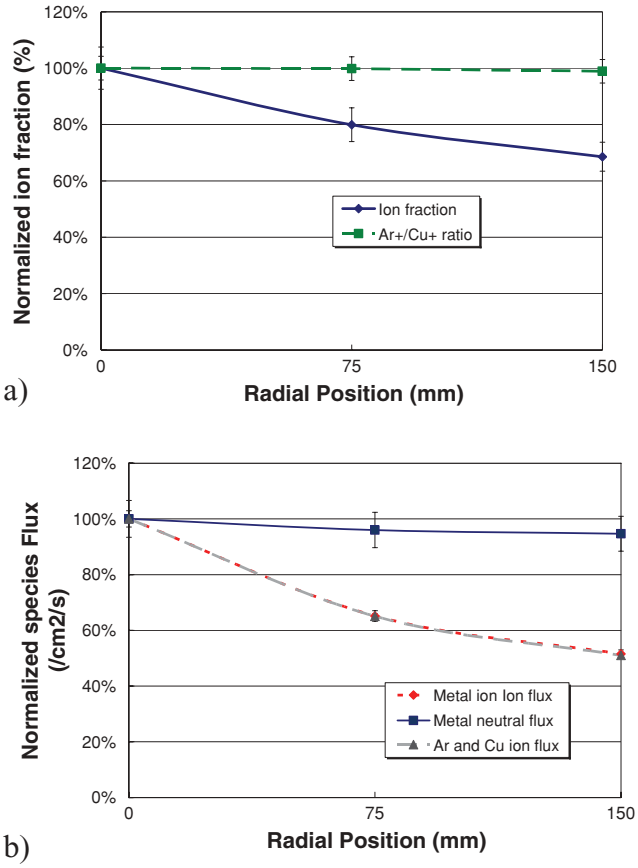

FIG. 5. (Color online) (a) Copper ion fraction and Cu^+/Ar^+ ratio. Copper ion fraction exhibits a center high spatial distribution. The Ar^+/Cu^+ ratio is a constant across the wafer. (b) Copper neutral, copper ion, and total ion flux measured by the QCM/GEA. Copper neutral deposition is uniform across the wafer, while both ion fluxes have domed profiles.

generated inside the target sheath (sputtering plasma) are accelerated back toward the sputter target. Only ions generated outside the target sheath have a chance to travel to the wafer. Typically, a sputtered metal neutral has a kinetic energy peak at a few electron volts, and has a high energy tail.[34] Hence, the majority of the ionized species typically have the relatively low energy inside the plasma because of the absence of electrical field there. Ions are accelerated by the voltage, $V_p - V_f$, and gain corresponding kinetic energy after entering sheaths created by plasma in the vicinity of any surfaces in contact with it. In the GEA, the ion energy distribution could be obtained by taking the derivative of the collected current with respect to the energy. The normalized ion energy distributions after the sheath acceleration at different locations are shown in Fig. 6. The ion energy distribution has a peak around 37 eV, which is slightly higher than $V_p - V_f$. The IED at the center and middle radius have a narrow distribution, while the edge has a broader distribution. The difference in distribution can be explained by the difference in the ion incident angle with respect to the sheath for the edge location. Ions enter the plasma sheath of the analyzer mesh more or less perpendicularly at the center and midradius positions, but enter it at the edge position at an angle of approximately 45°. It is due to the local shape of the magnetic field lines for the process conditions investigated in this experiment. The lines

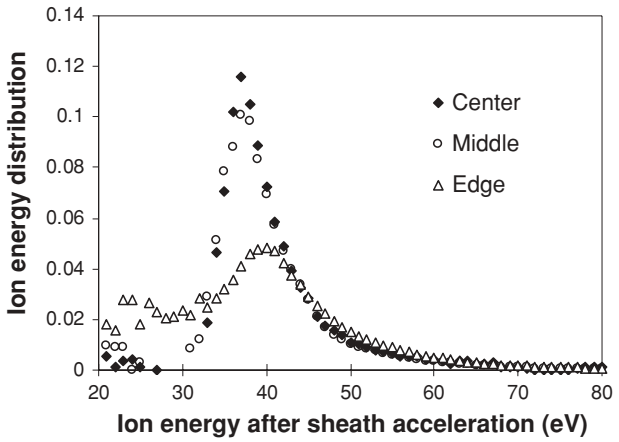

FIG. 6. After sheath acceleration, the IEDs at various radial positions. Ions at center and middle radius have narrow IED, while ions have broader IED at the edge due to the nonvertical magnetic field configuration.

cross the pedestal plane at this angle at the edge while they are normal to the pedestal at the center. The electrons follow the magnetic field lines under the influence of the Lorentz force. Ions, in turn, follow the electrons due to electrostatic attraction. Hence, ions enter the sheath of the edge analyzer mesh with some horizontal momentum. While they gain the

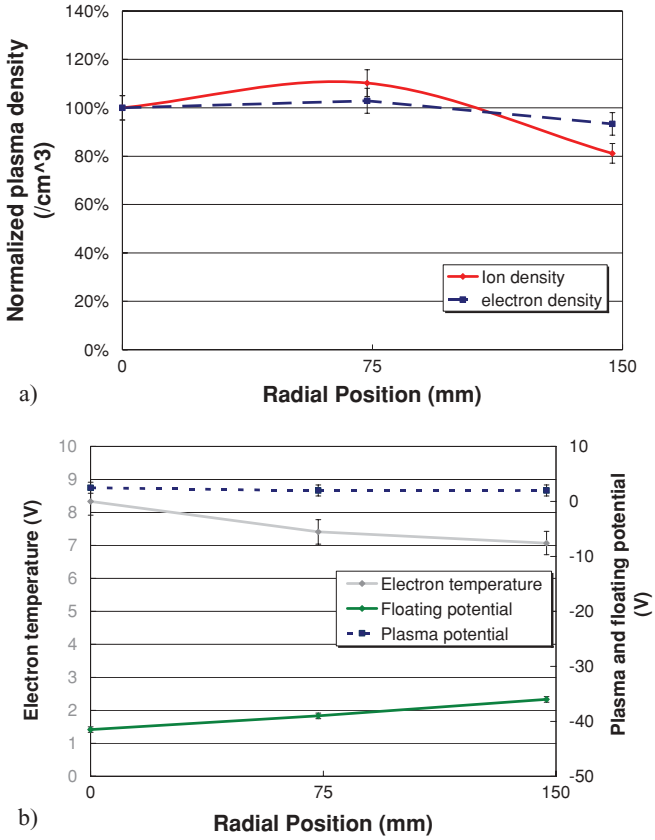

FIG. 7. (Color online) (a) Ion and electron densities obtained from 3 mm probes, indicating a domed ion density spatial profile. (b) Electron temperature, plasma potential, and floating potential at three radial positions corresponding to wafer center, midradius, and edge locations. Electron temperature is highest in the center. The V_f/T_e ratio is a constant of 5.

same kinetic energy, the momentum gain in the vertical direction will be less than in the case when they enter the sheath normal to the mesh. This effect artificially lowers the measured average ion energy and has to be taken into consideration when conclusions are made about $V_p - V_f$ at the edge location. High energy tails have been observed for all three positions.

C. Planar Langmuir probe data

Figure 7 shows the radial Langmuir probe measurements of ion and electron density on the wafer level for the same process as the one analyzed with QCM. The densities are normalized to the center probe's. The ion density is slightly higher than electron densities, which could be due to the effect of the presheath generated by the pedestal shield. The ion density has the domed profile across the wafer in which the center has 22% higher value. The corresponding ion flux calculated from the Langmuir probe data agrees well with the converted ion flux obtained from the GEA. The two methods agree to within 10% for the center position. The electron temperature at the center is 8.3 eV, which is higher than 7.1 eV measured at the edge. The floating potential exhibits the same trend as the electron temperature, and the ratio of V_f / T_e is 5 ± 0.2. The plasma potential, approximately 2 V higher than the ground potential, is spatially uniform across the wafer.

V. DISCUSSION AND CONCLUSIONS

Thickness measurement is the fast and most common way to characterize deposition and qualify process. However, it does not give any information about species ratios and energies across the wafer, which determine key process characteristics, such as step coverage, film continuity on sidewalls of recessed features, film quality, and overhang formation. Even worse, thickness measurements are often misleading when Ar and metal ions densities and energies are not uniform across the wafer.

In iPVD there are two competing film formation processes: film deposition by metal neutral and ion fluxes and film resputtering by gas and metal ions. The concurrent resputtering mitigates the final film thickness profile. The neutral deposition from the cup-shape HCM target is naturally uniform across the wafer in the range of 2% based on the line-of-sight deposition model.[35] The model data are in good correlation with our measurments for neutral flux as shown in Fig. 5(b). The metal ion flux (Fig. 5) at the edge is only ~50% of that at the center, which could result in very domed thickness profile if there is no sputtering. However, in the discussed case of HCM Cu deposition process, the difference in the film thickness between center and edge is only about 6%.[33] Partially it can be explained by the fact that neutrals comprise a large portion of the deposition flux. At the low operating pressure the sputtered copper neutrals reach the substrate virtually collision-free and are not affected by electrical or magnetic fields. The other important factor is an above mentioned film resputtering by the ion bombardment. The average ion energy (Fig. 6) is higher than the sputtering threshold. The Ar ion flux is higher than Cu ion flux, and both have the same domed flux profile. The resputtering by Ar and Cu ions, which happens concurrently with deposition, mitigates the effect of domed ion flux profile on film thickness. As a result, the Cu film with the good thickness uniformity is formed by the contribution of nonuniform deposition and sputtering fluxes across the wafer as in the presented case.

A comprehensive, combined plasma diagnostic method, including integrated QCM, GEA, and Langmuir probe, has been employed to map out the on-wafer plasma characteristics for a 300 mm HCM Cu source. The plasma density and temperature and floating potential were measured from Langmuir probe, while the metal fluxes, ion fraction, and Ar^+/Cu^+ ratios were determined by QCM. The ion energy and ion fluxes were obtained from GEA/QCM data. Characterization of these key plasma parameters leads to improved understanding of iPVD plasmas, enabling future development of HCM deposition processes for future technology generations.

[1] *The International Technology Roadmap for Semiconductors*, Semiconductor Industry Association (2007), http://public.itrs.net
[2] D. R. Juliano, D. N. Ruzic, M. M. C. Allain, and D. B. Hayden, J. Appl. Phys. **91**, 605 (2002).
[3] A. Sankaranand and M. J. Kushner, J. Vac. Sci. Technol. A **22**, 1242 (2004).
[4] V. Vyas and M. J. Kushner, J. Vac. Sci. Technol. A **24**, 1955 (2006).
[5] J. E. Foster, W. W. Wang, A. E. Wendt, and J. H. Booske, Proceedings of the IEEE International Conference on Plasma Science (Raleigh, NC, USA, 1998), p. 223.
[6] K. Okimura and T. Nakamura, J. Vac. Sci. Technol. A **21**, 988 (2003).
[7] I. Petrov, A. Myers, J. E. Greene, and J. R. Abelson, J. Vac. Sci. Technol. A **12**, 2846 (1994).
[8] Z. H. Barber, C. Christou, K.-F. Chiu, and A. Garg, Vacuum **69**, 53 (2002).
[9] S. M. Rossnagel and J. Hopwood, Appl. Phys. Lett. **63**, 3285 (1993).
[10] S. M. Rossnagel and J. Hopwood, J. Vac. Sci. Technol. B **12**, 449 (1994).
[11] K. M. Green, D. B. Hayden, D. R. Juliano, and D. N. Ruzic, Rev. Sci. Instrum. **68**, 4555 (1997).
[12] D. B. Hayden, D. R. Juliano, M. N. Neumann, M. C. Allain, and D. N. Ruzic, Surf. Coat. Technol. **120–121**, 401 (1999).
[13] J. W. Coburn, Thin Solid Films **171**, 65 (1989).
[14] S. G. Ingram and N. St. J. Braithwaite, J. Phys. D: Appl. Phys. **21**, 1496 (1988).
[15] E. A. Edelberg, A. Perry, N. Benjamin, and E. S. Aydil, J. Vac. Sci. Technol. A **17**, 506 (1999).
[16] C. Bohm and J. Perrin, Rev. Sci. Instrum. **64**, 31 (1993).
[17] J. Liu, G. L. Huppert, and H. H. Sawin, J. Appl. Phys. **68**, 3916 (1990).
[18] J. R. Woodworth, M. E. Riley, D. C. Meister, B. P. Aragon, M. S. Le, and H. H. Sawin, J. Appl. Phys. **80**, 1304 (1996).
[19] B. Lipschultz, I. Hutchinson, B. LaBombard, and A. Wan, J. Vac. Sci. Technol. A **4**, 1810 (1986).
[20] Z. Sternovsky and S. Robertson, Phys. Plasmas **11**, 3610 (2004).
[21] N. Hershkowitz, "How Langmuir probes works," in *Plasma Diagnostics*, edited by O. Auciello and D. L. Flamm (Academic, Boston, 1989), p. 113.
[22] D. N. Ruzic, *Electric Probe for Low Temperature Plasmas*, edited by W. Weed (The Education Committee American Vacuum Society, New York, 1994).
[23] F. F. Chen, *Plasma Diagnostic Techniques* (Academic, New York, 1965), p. 113.
[24] B. E. Cherrington, Plasma Chem. Plasma Process. **2**, 113 (1982).
[25] L. Schott, *Plasma Diagnostics* (Wiley, New York, 1968).
[26] J. D. Swift and M. J. Schwar, *Electrical Probes for Plasma Diagnostics* (American Elsevier, New York, 1970).
[27] S. M. Rossnagel and H. R. Kaufman, J. Vac. Sci. Technol. A **4**, 1822 (1986).
[28] S. M. Rossnagel and J. Hopwood, J. Vac. Sci. Technol B **12**, 449 (1994).

[29]S. M. Rossnagel, J. Vac. Sci. Technol. A **6**, 1821 (1988).
[30]See www.sycon.com, last accessed in Nov. 2009.
[31]W. J. Weber, R. J. Armstrong, and J. J. Trulsen, J. Appl. Phys. **50**, 4545 (1979).
[32]J. A. Hopwood, *Ionized Physical Vapor Deposition* (Academic, San Diego, 2000).
[33]A. Dulkin, E. Ko, L. Wu, I. Karim, K. Leeser, K.-J. Park, L. Meng, and D. N. Ruzic, *AVS 57th International Symposium and Exhibition*, October 17, 2010.
[34]*Sputtering by Particle Bombardment*, edited by R. Behrisch and W. Eckstein (Springer-Verlag, Berlin, 2007).
[35]R. Kinder, Unpublished data from Novellus' Computational Modeling.